Orbital
The electronic journal of chemistry

the electronic journal of chemistry

Full Paper | http://dx.doi.org/10.17807/orbital.v17i5.22789

Green Chemistry Approach to Corrosion Inhibition of Mild Steel in Acidic Medium Using *Myrica esculenta* Extract

Abhishek Sharma [a], Navneet Kaur [a], Manvinder Kaur [b], Rajeev Sharma [c], and Harvinder Singh Sohal*[a]

Corrosion of mild steel (MS) in acidic environments presents a significant challenge in industrial applications, often leading to structural degradation and economic losses. This study investigated the effectiveness of *Myrica esculenta* (ME) extract as a green corrosion inhibitor for MS in acidic media. A combination of methods—including weight loss experiments, contact angle measurements, surface analysis, and electrochemical techniques—was employed to evaluate the inhibitor's performance. In the absence of the ME inhibitor, MS experienced rapid corrosion and significant weight loss. However, the addition of ME extract, particularly at a concentration of 40 mg/L, markedly reduced corrosion, achieving an inhibition efficiency of 86.93% after 12 hours. Electrochemical polarization studies revealed a shift in corrosion potential toward more noble values, indicating a reduced tendency for corrosion. Adsorption studies suggested that the inhibitor formed a protective layer through both monolayer and possible multilayer adsorption mechanisms. Contact angle analysis showed an increase in surface hydrophobicity, confirming the formation of a protective interface layer. UV analysis further validated the presence of this layer, which played a crucial role in minimizing pitting and preserving the structural integrity of the mild steel surface. These findings underscore the potential of ME as an effective and environmentally benign corrosion inhibitor.

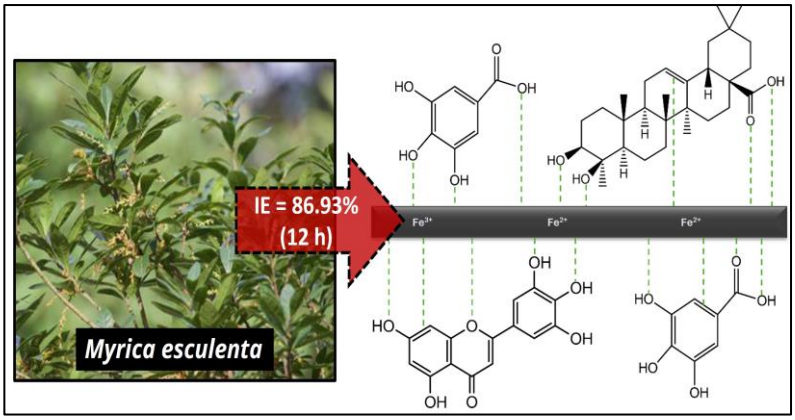

Keywords

Myrica Esculenta
Green corrosion inhibition
Electrochemical analysis
Adsorption isotherms
Protective coating
Polarization studies

Article history

Received 25 Apr 2025
Accepted 29 Nov 2025
Available online 06 Dec 2025

Handling Editor: Marcos S. Amaral

1. Introduction

Corrosion, is defined in the ISO 8044 standard, is the corrosion of metals caused by their physicochemical contact

[a]Department of Chemistry, Chandigarh University, Gharuan-140413, Mohali, Punjab, India. [b]Chitkara University Institute of Engineering and Technology, Chitkara University, Rajpura-140401, Punjab, India. [c]Department of Chemistry, M. M. Modi College, Patiala-147001, Punjab, India. *Corresponding author. Email: **drharvinder.cu@gmail.com**

with the surrounding environment or the technical systems into which they are integrated [1]. It basically refers to a material's spontaneous and natural degradation brought on by chemical or electrochemical assaults, which are caused by metals' intrinsic instability. Corrosion leads to the loss or alteration of the properties that initially made the material suitable for specific applications. Therefore, selecting the correct material is crucial to mitigate or avoid this technological, safety, economic, and environmental issue [2]. According to Kirmeyer *et al.*, water utilities in the USA replace approximately 0.6% of their water mains annually, primarily due to aging infrastructure. They found that in 1992, it was estimated that 48% of water pipes were made of spun cast iron, with an additional 19% composed of ductile iron, highlighting their vulnerability to corrosion. According to recent statistics, water utilities in Australia use approximately 260,000 km of buried pipelines, with more than 70% made of ferrous metal. With a population of 22 million, critical transmission mains, which generally span 150,000 km, are composed of ferrous metal [3].

Corrosion has outstanding impact on the environment, and its inhibition has been extensively studied [4]. Corrosion inhibitors are among the most widely used techniques of corrosion control and prevention [5, 6]. Corrosion inhibitors effectively limit destructive effects and prevent metal disintegration. Inhibitors are crucial for preventing corrosion of metals and alloys exposed to harsh environments. Inhibitors introduced at low concentrations to corrosive media reduce metal dissolution and restrict adsorption on metal surfaces [7, 8]. Corrosion inhibitors primarily reduce corrosion by adsorbing onto surfaces and forming protective layers and can be broadly classified into two categories inorganic and organic types. The mild steel surface is oxidized and isolated by inorganic inhibitors, whereas heteroatoms or double bonds are used by organic inhibitors. Organic inhibitors create interfacial bonds by donating electrons to metal atoms with vacant orbitals. However, organic inhibitors are environmentally hazardous and pose significant risks to human health [9].

India's traditional medicines including Unani, Siddha, Homeopathy, and Ayurveda, have been practiced since ancient times. Plants have been utilized for centuries to sustain human health and provide medicinal ingredients in modern pharmacopoeias [10]. Plant extracts have demonstrated their effectiveness as eco-friendly anti-corrosion agents for steel. These extracts contain phytochemicals rich in heteroatoms—such as oxygen, nitrogen, phosphorus, and sulfur—as well as various linkages that facilitate their adsorption onto the surface of steel [11]. The dioecious, tiny, evergreen tree is called Myrica esculenta (*M. esculenta*). Located in the mountain ranges from Ravi eastward to Assam, as well as in Arunachal Pradesh, Meghalaya, Sikkim, Assam, Nagaland, Manipur, and Mizoram in Khasi, Jaintia, Kamarupan, and the Lushai hills at a height of 900–2100 meters, it is indigenous to the Republic of India [12].

M. esculenta, widely known as Kaphal plants, additionally known as Himalayan bayberry, Kaiphal, Kaphal, Maruta, and Kefang, belongs to family of *myricaceae* [13, 14]. This medium to big evergreen tree may reach a height of 12-15 meters and has a trunk girth of 92.5 centimeters. The bark can vary from light brown to black, and the leaves are lanceolate, ovate, or serrate. They cluster around the ends of branches [15]. *M. esculenta* belong to the *Myrica* genus. This genus contains 97 species (Sood & Shri, 2018) of small trees of a medium height of 20–25 ft [16]. *M. esculenta* is abundant in the Himalayan regions and has significant socio-economic value. The herb is known for its therapeutic benefits.

M. esculenta has traditionally been highly beneficial. It has therapeutic properties for ulcers, anemia, pyrexia, diarrhea, cough, and ENT infections [17]. Myricitrin, a chemical discovered in *M. esculenta*, is responsible for various biological actions. *M. esculenta* is a unique species within the *Myrica* genus found exclusively in India [18]. As a nitrogen-fixing plant, it helps restore nitrogen-depleted soils. Its fruits, highly valued in the sub-Himalayan region for their exceptional taste, are known for their nutritional and therapeutic benefits. Commercially, *M. esculenta* relies entirely on wild collections by indigenous people. This dependence has endangered the species due to urbanization, over-harvesting, unsustainable practices, and over-exploitation of forests and wastelands. High levels of human activity also hinder natural regeneration, threatening the plant's population [19].

M. esculenta is well-recognized in Ayurvedic and Unani medicine. Its fruits and roots are used in Ayurvedic formulations like Brahmarasayan and Chyawanprash. The leaves of this plant are lanceolate, ovate, or serrate and cluster at the terminals of the branches. The blossoms are supposed to heal earaches, paralysis, and diarrhea, while the roots have been used for asthma, cholera, and bronchitis [15, 20]. Research was done to commence a domestication program for the medicinally essential fruit tree *M. esculenta*, with the goal of examining variety in fruit and seed properties. The plant's versatility has led to overexploitation and a lack of sustainable methods, significantly impacting its natural regeneration. Consequently, the scope of study is to assess the collision of human activities on population dynamics and regeneration capacity of *M. esculenta* within the subtropical mixed pine forests of Meghalaya [20].

2. Material and Methods

2.1 Materials

M. esculenta (ME) leaves were sourced from the outskirts of Saharan in Himachal Pradesh. The research region spans 31°49'51.24"N latitude and 77°16'59.88"E longitude, with elevations ranging from 250 to 7415 m. Sulphuric acid, acetone, and methanol obtained from Sigma Aldrich, were used directly without any additional purification steps. The experiment utilized borosilicate glassware, including a round-bottom flask and a Soxhlet apparatus. Methanol was utilized as the solvent for the extraction, which was evaporated using a rotary evaporator (SARE-T43). The electrochemical experiments were performed using a Metrohm Autolab electrochemical analyzer (Model PGSTAT102) with Nova 2.1 software. UV-visible spectrophotometric analysis was conducted using a UV-Vis spectrophotometer (Model 1900, Chandigarh University). Scanning electron microscopy (SEM) was carried out using a JEOL scanning electron microscope (Model JSM-6100, Punjab University).

2.2 Preparation of Plant Extract

The *M. esculenta* plant leaves were meticulously washed multiple times by using distilled water to separate out dirt and external impurities. The cleaned leaves were air-dried in the shade for 7 days during July (at an ambient temperature of 35°C) to prevent moisture retention and fungal growth. Once dried, the leaves were ground into a coarse powder, and 50 g of the powdered material was carefully placed inside a thimble. Soxhlet extraction was carried out using

approximately 250 mL of methanol as the solvent at a reflux temperature of 80°C for 12 hours. The solvent was subsequently evaporated utilize a rotary evaporator, yielding 6 g of crude extract. The resulting extract was securely stored in stock vials and kept in a refrigerator at 4–6°C for future analysis or experimental use.

2.3 Preparation of Mild Steel Coupons

Mild steel (MS) sheets, sourced from Gobindgarh, Punjab (30°40'58.0872'' N, 76°17'39.1632'' E), were analyzed to have 0.20 wt% carbon, 0.48 wt% manganese, 0.18 wt% silicon, 0.039 wt% phosphorus, 0.03 wt% sulfur, and the remainder iron. The sheets were polished with sandpapers (200–2000 grit) to remove impurities and ensure smooth surfaces, then marked into 1 × 1 cm sections and cut into uniform coupons. Further polishing standardized their edges and weights, ensuring consistency in surface area and mass. The coupons were cleaned with acetone to eliminate contaminants, dried to prevent oxidation, and stored them for further analysis or experimentation.

2.4 Preparation of Working Electrode

The working electrode were created using an MS specimen with measurements of 1 cm × 1 cm × 5 cm. The steel surface was embedded in epoxy resin, ensuring that only 1 cm² was exposed for electrochemical analysis. The exposed surface was polished sequentially with sandpaper up to 1200 grit to achieve a smooth finish. After polishing, the surface was thoroughly rinsed with double-distilled water and degreased using acetone. Corrosion studies were then conducted under open-air, non-stirring conditions with different concentrations of the inhibitor. Experiments involving electrochemistry were conducted utilizing a three-electrode configuration linked to an electrochemical workstation. In this setup, Platinum wire was used as the counter electrode, a saturated calomel electrode (SCE) as the reference electrode, and the MS sample as the working electrode, as shown in **Figure 1**.

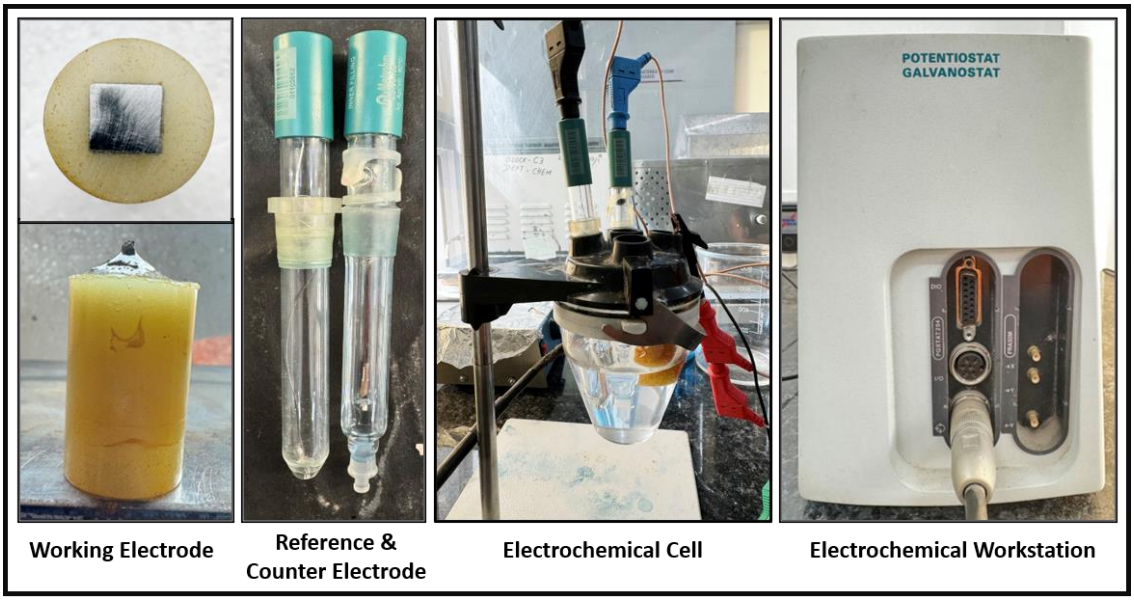

Fig. 1. A schematic depiction of a working, reference, and counter electrodes, as well as the electrochemical cell and workstation configuration.

2.5 Weight Loss Measurements

The capability of the inhibitor in weight loss measurements was evaluated by determining the weight loss of MS coupons. This process involved recording the weight of the MS coupons with and without immersed in 50 mL of 1 M H_2SO_4 solution, both before and after the ME inhibitor at varied amounts (10, 20, 30, and 40 mg/L) and exposure durations (12, 24, and 48 hours). Before each experiment, the MS coupon surfaces were polished with sandpaper of various grit levels to achieve a homogeneous surface. Weight loss data was utilized to quantify corrosion rate (CR) inhibition efficiency (IE), surface coverage (θ), and by **equations 1–3**, as described in previous studies.

$$CR\ (mg\ cm^{-2}\ h^{-1}) = \frac{k \times \Delta W}{D \times A \times T} \quad (1)$$

$$IE\ (\%) = \frac{W_0 - W_i}{W_0} \times 100 \quad (2)$$

$$\theta = \frac{W_0 - W_i}{W_0} \quad (3)$$

where the weight loss, denoted as ΔW, is the difference between the initial weight (W_0) and the weight in the presence of the ME inhibitor (W_i), both measured in milligrams (mg). The surface coverage is represented by θ, k is the corrosion constant *i.e.,* 534, D refers to the density of the MS coupon (in g/cm³) *i.e.,* 7.85 g/cm³ for MS, A is the total surface area of the steel coupon (in cm²), and T is the duration of corrosion (in hours) [21]. All experiments were performed in triplicate in order to ensure reproducibility.

2.6 Electrochemical Measurements

The MS coupons were analyzed through electrochemical studies using a Metrohm Autolab (Model PGSTAT 102) controlled by Nova 2.1 software, which included both Electrochemical impedance spectroscopy (EIS) and potentiodynamic polarization (PDP) testing. The corrosion cell had three electrodes a saturated calomel reference electrode, a platinum counter electrode, and an MS working electrode. Electrochemical experiments were conducted using a single perturbation amplitude of 5 mV at the open-circuit potential (OCP) and a scan rate of 0.05 mV/s, throughout a frequency range of 100 kHz to 0.01 Hz. At the

same scan rate, potentiodynamic polarization curves were acquired, running from -250 mV in relation to the OCP to +250 mV in relation to the saturated calomel electrode (SCE). Before each experiment, the working electrode was immersed in a 1 M H_2SO_4 solution for around 45 minutes to make sure it entered a stable condition and establish the OCP. The inhibition efficiency of the corrosion inhibitor was calculated using **equation 4**,

$$IE\ (\%) = \frac{I_{0corr} - I_{icorr}}{I_{0corr}} \times 100 \qquad (4)$$

The corrosion current densities are shown by the symbols I_{0corr} and I_{icorr}, respectively, when the ME inhibitor is present and absent. To stabilize the OCP before to experimentation, the working electrode was submerged in the acidic solution for forty-five minutes. The effectiveness of inhibition was calculated using **equation 5**,

$$IE\ (\%) = \frac{R_{ct} - R^0_{ct}}{R_{ct}} \times 100 \qquad (5)$$

where R_{ct} and R^o_{ct} represent the charge transfer resistance in the presence and absence of the ME inhibitor, respectively. All experiments were performed in triplicate in order to ensure reproducibility [22].

2.7 Adsorption isotherm analysis

To investigate corrosion inhibition processes, the Langmuir and Freundlich adsorption isotherm models are frequently employed. Adsorption on a surface with a finite number of uniform sites is assumed by the Langmuir isotherm, each capable of holding a single inhibitor molecule, resulting in monolayer adsorption without interactions between the adsorbed molecules. This model indicates strong and uniform adsorption on a homogeneous surface if the inhibitor is well-suited. Conversely, the Freundlich isotherm describes adsorption on heterogeneous surfaces with varying site energies, allowing for both monolayer and multilayer adsorption. It is particularly relevant for uneven steel surfaces, where adsorption intensity varies across different sites. Analyzing experimental data using these models helps determine the nature of adsorption, whether it forms a monolayer or multilayer, and whether the surface is homogeneous or heterogeneous, offering insights into the corrosion inhibition mechanism and efficiency [23].

2.8 UV Characterization

To look at how iron cations (Fe^{2+} and Fe^{3+}) interact with t he chemicals that inhibit ME extract, UV spectrophotometry was conducted using a Shimadzu UV-Vis spectrophotometer (Model 1900, Chandigarh University) over a wavelength range of 200–800 nm. Prior to and following a 24-hour immersion of a mild steel chip in 1M H_2SO_4 containing 400 ppm of the inhibitor, the ME extract solution was examined. Shifts in the absorption maximum (λ_{max}) and changes in absorbance intensity were examined to detect potential inhibitor-iron complex formation. Variations in spectral features, such as new peak appearances, peak shifts, or intensity changes, indicated interactions between the active phytochemicals in ME and iron cations, supporting the proposed mechanism of inhibition. These findings are elaborated in the results and discussion section. All experiments were performed in triplicate in order to ensure reproducibility [24].

2.9 Contact angle analysis

The surface qualities of mild steel coupons were assessed under various situations using water contact angle analysis. To establish a baseline, a freshly polished coupon's first contact angle was measured. Subsequently, the contact angle of coupons submerged in 1M H_2SO_4 without the ME inhibitor was recorded to assess the effects of acidic corrosion on the surface. Additionally, the contact angle of coupons immersed in 1M H_2SO_4 with the inhibitor was measured to illustrate the inhibitor's effectiveness in preserving or improving hydrophobicity in corrosive conditions. All measurements were conducted using Ossila contact angle software, with each calculation repeated three times for accuracy. All experiments were performed in triplicate in order to ensure reproducibility.

2.10 Surface Analysis

The SEM analysis was performed using a Joel JSM-6100 model, offering high magnification and resolution (up to 40 Å) to examine surface morphology. Using this method, the surface of MS coupons was examined both before and after the inhibitor, before to and during immersion in a 1 M H_2SO_4 solution. To stop additional air corrosion, the MS coupons were taken out of the solution after weight loss measurements, washed with distilled water to get rid of any remaining acid or inhibitor, and then dried in a desiccator. Prior to analysis, the MS coupons were thoroughly cleaned, polished to a mirror-like finish, and degreased with acetone to remove surface impurities. Following immersion in the acidic solution, the coupons was again wash with distilled water to take out any remaining acid or inhibitor and dried in a desiccator to avoid oxidation [25].

3. Results and Discussion

3.1 Phytochemical screening of *Myrica esculenta* plant

Phytochemical analysis of *Myrica esculenta* extract revealed the presence of several bioactive compounds, confirmed through various standard tests, as summarized in **Table 1**. Alkaloids were identified using Mayer's, Wagner's, Dragendroff's, and Hager's tests, all showing positive results with yellow cream, brown-reddish, red, and yellow precipitates, respectively. Phytosterols were confirmed through Salkowski's, Libermann Burchard's, and Tshugajeu tests, producing golden yellow color, brown ring at the junction of layers, and eosin red color, respectively [10].

Carbohydrates were detected by Molish's and Fehling's tests, showing a violet ring and red precipitate, respectively. Glycosides were confirmed through Legal's and modified Bontrager's tests, with pink color and rose-pink line, respectively. Saponins were identified by the Froth and Foam tests, both showing foam formation. Oils and fats were detected by the stain test, where an oily stain formed on paper [26].

Phenolic compounds were confirmed through the Ferric chloride test, yielding a bluish-black color. Tannins were detected by the Gelatin test, which produced a white precipitate. Triterpenes were identified by the Copper acetate test, resulting in a green color. Proteins were confirmed by Biuret, Ninhydrin, and Xanthoproteic tests, showing purple-violet, blue, and yellow colors, respectively. Flavonoids were detected by Zinc hydrochloride acid reduction, Shinoda, and Lead acetate tests, all producing magenta color and yellow precipitates. These results indicate that *M. esculenta* extract contains a diverse range of bioactive compounds, supporting its potential as a natural source of medicinal agents.

Table 1. Phytochemical constituents screening of *Myrica esculenta* extracted using methanol.

Phytochemical constituents	Tests for determination	Literature results	Experimental results	Reference
Alkaloids	Hager's test	Present	Present	[26]
	Wagner's test	Present	Present	[26]
	Dragendroff's test	Present	Present	[26]
	Mayer's test	Present	Present	[10]
Phytosterols	Salkowski's test	Present	Present	[10]
	Libermann Burchard's test	Present	Present	[26]
	Tshugajeu test	Present	Present	[10]
Carbohydrates	Molish's test	Present	Present	[26]
	Fehling's test	Present	Present	[10]
Glycosides	Legal's test	Present	Present	[10]
	Modified Bontrager's test	Present	Present	[26]
Saponins	Froth test	Present	Present	[26]
	Foam test	Present	Present	[26]
Oils and fats	Stain test	Present	Present	[10]
Phenols	Ferric chloride test	Present	Present	[26]
Tannins	Gelatin test	Present	Present	[10]
Triterpenes	Copper acetate test	Present	Present	[26]
Proteins	Biuret test	Present	Present	[10]
	Ninhydrin test	Present	Present	[10]
	Xanthoproteic test	Present	Present	[10]
Flavonoids	Zinc hydrochloride acid reduction test	Present	Present	[26]
	Shinoda test	Present	Present	[10]
	Lead acetate test	Present	Present	[26]

3.2 Weight loss measurements

A detailed examination of MS corrosion behaviour in 1 M H_2SO_4 solutions with non-identical doses of the ME inhibitor revealed considerable increases in corrosion resistance. The corrosion parameters, including weight loss, inhibition efficiency, and corrosion rate, were assessed at intervals of 12, 24, and 48 hours, as shown in **Table 2**. These results enhance the effectiveness of the ME inhibitor in mitigating the corrosive effects of the acidic environment. The study involved measuring the weight of MS coupons before and after concentration in 50 mL of 1 M H_2SO_4 solution, with and without the ME inhibitor, at concentrations of 10, 20, 30, and 40 mg/L, over the specified durations.

Table 2. Weight loss measurements of MS in 1 M H_2SO_4 solution with varying concentrations of ME inhibitors at 303 K.

Time (h)	Conc. (mg/L)	Initial weight, W_0 (g)	Final weight, W_i (g)	Weight loss, ΔW (g)	Surface coverage (θ)	Inhibition efficiency (%)	Corrosion Rate (mg/cm²/h)
12	0	4.101±0.005	3.045±0.001	1.056±0.003	-	-	2.00
	10	4.087±0.001	3.522±0.003	0.565±0.001	0.4650	46.50	1.07
	20	4.114±0.003	3.775±0.002	0.339±0.001	0.6790	67.90	0.64
	30	4.175±0.004	3.971±0.001	0.204±0.002	0.8068	80.68	0.39
	40	4.109±0.001	3.971±0.005	0.138±0.003	0.8693	86.93	0.26
24	0	3.045±0.002	1.798±0.001	1.247±0.005	-	-	2.36
	10	3.522±0.001	2.798±0.003	0.724±0.001	0.4194	41.94	1.37
	20	3.775±0.003	3.2998±0.002	0.4752±0.003	0.6189	61.89	0.90
	30	3.971±0.001	3.598±0.003	0.373±0.002	0.7009	70.09	0.70
	40	3.971±0.008	3.714±0.001	0.257±0.003	0.7939	79.39	0.49
48	0	1.798±0.003	0.511±0.006	1.287±0.004	-	-	2.43
	10	2.798±0.001	1.902±0.005	0.896±0.001	0.3038	30.38	1.69
	20	3.2998±0.003	2.602±0.001	0.6978±0.008	0.4578	45.78	1.32
	30	3.598±0.001	3.102±0.003	0.496±0.003	0.6146	61.46	0.94
	40	3.714±0.002	3.353±0.002	0.361±0.007	0.7195	71.95	0.68

Using varying dosages of the ME inhibitor, the corrosion behaviour of MS in 1 M H_2SO_4 solution was investigated in detail throughout exposure durations of 12, 24, and 48 hours at 303 K. In the absence of the inhibitor, the corrosion rate was quite high. The blank MS coupon saw substantial weight loss, suggesting extensive deterioration owing to the hostile acidic media. However, as the ME inhibitor concentration increased, a marked reduction in the corrosion rate was observed. At the highest concentration (40 mg/L) of ME inhibitor, the corrosion rate significantly decreased from 2.00 mg/cm²/h to 0.26 mg/cm²/h within 12 hours, highlighting the strong protective effect of the inhibitor. This trend continued over 24 and 48 hours, where the corrosion rates remained significantly lower than the untreated sample, reflecting the strong protective nature of the inhibitor.

As expected, the IE and surface coverage both increased with the concentration of the inhibitor, reaching a maximum at 40 mg/L. At 12 hours, the inhibition efficiency at this concentration was 86.93%, which gradually reduced to 71.95% by 48 hours, indicating that while the inhibitor provided strong initial protection, its effectiveness gradually decreased over time. The decrease in IE over longer exposure times is typical, as the inhibitor may slowly desorb from the surface or react with the acidic solution. Nonetheless, even after 48 hours, the inhibitor still provided over 70% efficiency, showing its effectiveness for extended periods. The surface coverage

followed a similar pattern, with larger inhibitor concentrations resulting in increased surface coverage, confirming ME molecule binding onto the MS surface and their involvement in blocking active sites that would otherwise react with the acid.

The results demonstrate that the protective effect of the inhibitor was most evident at higher concentrations, where it effectively reduced the corrosion rate, minimized weight loss, and maintained a substantial inhibition efficiency over the 48-hour exposure period. While the effectiveness of the inhibitor diminished slightly over time, it still provided valuable protection, positioning ME as in bright corrosion inhibitor for use in acidic environment. These findings not only highlight the inhibitor's potential for practical applications but also suggest its ability to mitigate corrosion effectively in real-world scenarios, ensuring the permanency and durability of metal surfaces exposed to corrosive conditions. The variation in corrosion inhibition efficiency between different batches of the same plant extract highlights the challenges of standardization due to natural variability in phytochemical composition.

3.3 Electrochemical measurements

3.3.1 Electrochemical impedance spectroscopy measurements

The measurements of EIS were carried out at 303 K to assess the impedance properties of MS in 1 M H_2SO_4 with varying ME inhibitor doses. The change in potential of MS (as opposed to SCE) over time in the aerated acidic solution containing the inhibitor is shown in **Figure 2b**. Quickly, a steady potential was reached, which matched MS's free corrosion potential (E_{corr}). Before every experiment, the working electrode was immersed in the solution for 600 seconds at 303 K to give the potential time to settle. After 600 seconds, the open-circuit potential (OCP) reached a nearly constant value, indicating the establishment of a steady state, [27] as seen in **Figure 2b**. All measurements were performed under constant temperature conditions at 303 K. **Figure 2a** shows how the inhibited and uninhibited systems are analyzed using the electrical equivalent circuit concept. The solution resistance in this circuit is represented by R_s, the charge transfer resistance by R_{ct}, and the double-layer capacitance by C_{dl}.

The corrosion parameters assessed involves resistance solution (R_s), resistance in charge transfer (R_{ct}), resistance polarization (R_p), capacitance in double-layer (C_{dl}), and inhibition efficiency (IE), are represented in **Table 3**. The Nyquist plot in **Figure 3** displays the impedance response, featuring a series of semicircles with increasing diameters as the immersion of the ME inhibitor increases. The behavior suggests enhanced corrosion resistance, which can be ascribed to the formation of a protective film by the ME inhibitor on the MS surface. This protective film effectively increases the resistance in charge transfer, thereby reducing the corrosion rate and mitigating the degradation of the material.

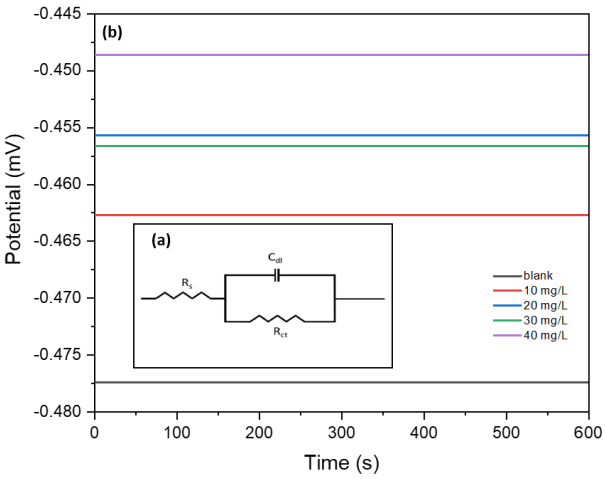

Fig. 2. (a) The impedance response of MS in a 1 M H_2SO_4 solution, with and without the ME inhibitor, was simulated at 303 K using an electrical equivalent circuit. (b) The ME inhibitor stabilizes the MS OCP at 303 K, as demonstrated by the time curves for the OCP in 1 M H_2SO_4 solution.

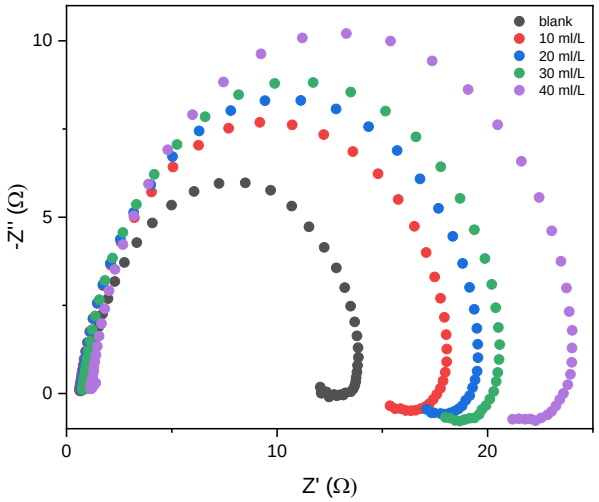

Fig. 3. Nyquist plot for MS in 1 M H_2SO_4 solution presence and absence different ME inhibitor doses (10, 20, 30, and 40 mg/L) at 303 K.

Table 3. EIS parameters for MS in 1 M H_2SO_4 with and without various concentrations 10, 20, 30, and 40 mg/L of ME inhibitor at 303K.

Inhibitor concentration (mg/L)	R_s (Ω)	R_{ct} (Ω)	R_p (Ω)	C_{dl} (F)	IE (%)
0	1.121	10.931	12.052	0.001715	-
10	0.834	14.534	15.368	0.001747	34.79
20	0.903	16.202	17.105	0.000883	52.53
30	1.003	16.989	17.992	0.000799	75.66
40	1.392	19.796	21.188	0.000605	80.78

The R_{ct} value of 10.931 Ω in uninhibited 1 M H_2SO_4 solution indicates a significant rate of charge transfer and corrosion activity on the MS surface. The corresponding R_p value was 12.052 Ω, reflecting low polarization resistance, while the C_{dl} was 0.001715 F, which is characteristic of a highly exposed metal surface with minimal protection. These parameters underscored the aggressive corrosive nature of the acidic medium in the absence of any inhibitor.

The introduction of the ME inhibitor led to a notable improvement in the corrosion resistance of MS. With increasing inhibitor concentrations, the R_{ct} values

progressively increased, reaching a supreme of 19.796 Ω at 40 mg/L. The considerable increase in R_{ct} showed a robust inhibitory effect, attributable to the invention of an adsorbed protective layer of the molecules that inhibit on the metal surface. Similarly, the R_p values increased correspondingly, peaking at 21.188 Ω for 40 mg/L, further validating the inhibitor's ability to suppress corrosion.

The decline in C_{dl} values was notice as the inhibitor concentration increased, with the highest concentration (40 mg/L) showing the lowest C_{dl} value of 0.000605 F. This reduction in C_{dl} indicated a decrease in the susceptible metallic surface area due to the adsorption of inhibitor molecules. The formation of a robust inhibitor film led to a diminished dielectric constant and increased double-layer thickness, enhancing the corrosion resistance of MS.

The IE calculated from R_{ct} values demonstrated a consistent improvement with higher inhibitor concentrations. At 10 mg/L, the IE was 34.79%, which increased to 80.78% at 40 mg/L. The ME inhibitor effectively reduces corrosion by covering a large surface area and forming a protective barrier, improving MS corrosion resistance. **Figure 4** shows Bode graphs of MS submerged in 1 M H_2SO_4 solution in presence and absence of different doses (10, 20, 30, and 40 mg/L) of ME inhibitor at 303 K. The phase angle and impedance modulus charts demonstrate how the inhibitor affects corrosion resistance. The impedance response improves with increasing inhibitor concentration, suggesting improved corrosion prevention.

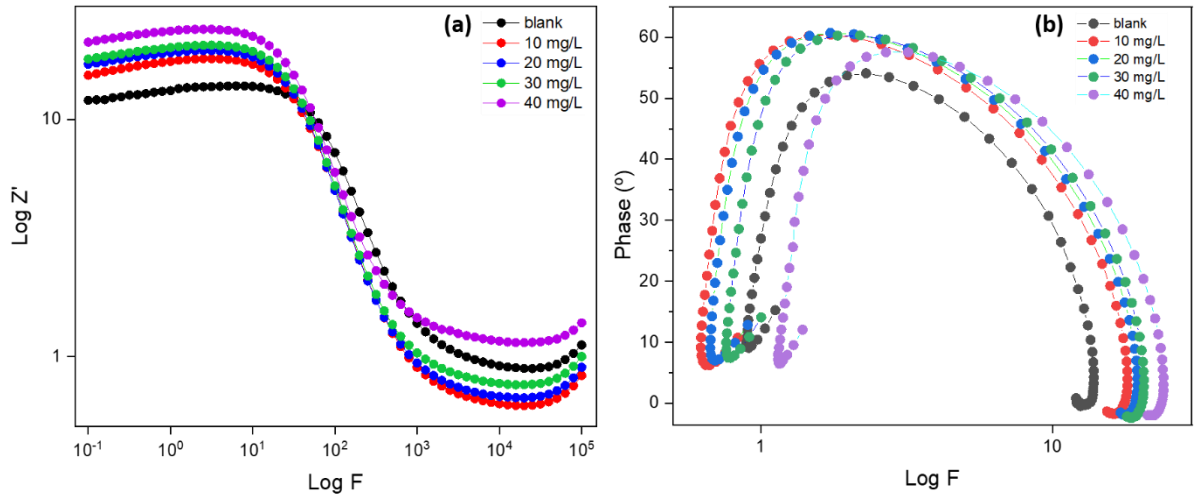

Fig. 4. Bode graphs for MS at 303 K in the 1 M H_2SO_4 solution in presence and absence of different ME inhibitor doses (10, 20, 30, and 40 mg/L).

The data highlight the effectiveness of the ME inhibitor in protecting MS in acidic environments. The observed increase in R_{ct} and R_p values, alongside a reduce in C_{dl} and a rise in inhibition efficiency, confirms the inhibitor's ability to adsorb onto the MS surface, thereby significantly improving its corrosion resistance. These results emphasize the potential of the ME inhibitor as an efficient corrosion protection agent in acidic conditions, offering a promising solution for various industrial applications. A gradual decline in inhibition efficiency over the exposure period suggests that the active phytochemicals in the plant extract may undergo degradation or desorption from the metal surface, thereby reducing the protective barrier and limiting its long-term effectiveness.

3.3.2 Photodynamic polarization measurements

The electrochemical polarization parameters for MS in the 1 M H_2SO_4 solution, both presence and absence of different concentrations (10, 20, 30, and 40 mg/L) of the ME inhibitor at 303 K, are detailed in **Table 4** and illustrated in **Figure 5**. These parameters encompass corrosion potential (measured in volts vs. SCE), I_{corr}, anodic and cathodic Tafel slopes (βa and -βc), CR, and IE. The findings provide essential insights into the corrosion behavior of MS when exposed to the ME inhibitor, demonstrating its significant ability to reduce corrosion rates and enhance the material's durability against degradation in acidic conditions.

Table 4. MS polarization characteristics in 1M H_2SO_4 with and without different concentrations of ME inhibitor (10,20,30, and 40mg/L) at 303k.

Inhibitor concentration (mg/L)	E_{corr} (V vs. SCE)	I_{corr} (A/cm)	R_p (Ω)	β_a (V/dec)	$-\beta_c$ (V/dec)	CR (mg/cm²/h)	IE (%)
0	-0.471	1.00×10^{-4}	125.31	0.111	0.039	0.069	-
10	-0.457	2.12×10^{-5}	1131.54	0.134	0.084	0.0342	50.42
20	-0.448	2.58×10^{-5}	1074.80	0.163	0.105	0.0217	68.63
30	-0.421	3.14×10^{-6}	1223.65	0.195	0.152	0.0178	74.25
40	-0.409	4.96×10^{-6}	934.67	0.224	0.204	0.0146	78.81

The study examines how MS corrodes in 1 M H_2SO_4 at 303 K both with and without the addition of different ME inhibitor doses (10, 20, 30, and 40 mg/L). The results show a marked improvement in corrosion resistance with the presence of the inhibitor, demonstrating its effectiveness in reducing corrosion rates and enhancing the protective properties of the material in acidic environments. The E_{corr} moves slightly to less negative values, showing that the ME inhibitor functions

as a mixed-type inhibitor, lessening both anodic dissolution of metal and cathodic hydrogen evolution processes. The I_{corr} decreased from 1.00×10−4 A/cm² (uninhibited) to 4.96×10−6 A/cm² at 40 mg/L, confirming the inhibitor's efficiency in lowering corrosion activity. The polarization resistance (R_p) improves from 125.31 Ω to 934.67 Ω, indicating improved corrosion resistance from inhibitor adsorption on the MS surface.

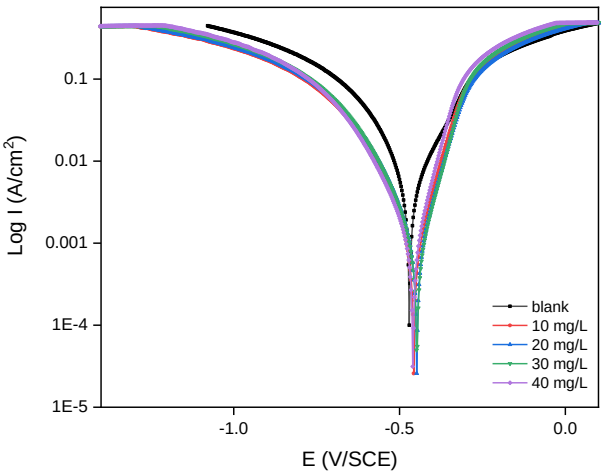

Fig. 5. Tafel plots for MS in 1 M H_2SO_4 solution in presence and absences of various concentrations 10, 20, 30, and 40 mg/L of ME inhibitor at 303K.

Increasing inhibitor concentration leads to considerable increases in Tafel slopes (βa and −βc), suggesting suppression of anodic and cathodic reactions. The CR decreases significantly from 0.069 mg/cm²/h in the uninhibited solution to 0.0146 mg/cm²/h at 40 mg/L of inhibitor, demonstrating a substantial reduction in material degradation. This drop-in corrosion rate is directly proportional to the inhibitor's efficiency in lowering corrosion current. The IE gradually increases from 50.42% at 10 mg/L to 78.81% at 40 mg/L, indicating that greater inhibitor doses provide superior corrosion protection. These findings suggest that the ME inhibitor forms a stable adsorption layer on the MS surface, blocking active corrosion sites and significantly reducing material degradation. The inhibitor's effectiveness increases with concentration, reaching optimal inhibition efficiency at 40 mg/L. It works by a mixed-type mechanism, increasing corrosion resistance by reducing both anodic and cathodic processes. As a result, the ME inhibitor is very efficient in improving the corrosion resistance of MS in acidic conditions, making it an attractive choice for industrial applications. The reduction in corrosion inhibition over extended exposure indicates that the plant-based inhibitor may lack the durability required for prolonged protection, potentially due to the breakdown of bioactive compounds or insufficient adsorption stability on the metal surface.

3.4 Adsorption isotherm analysis

The study of corrosion inhibition is critical for enhancing the durability and performance of MS in aggressive environments, such as acidic solutions. This research explores the adsorption characteristics of the ME inhibitor on MS surfaces immersed in 1 M H_2SO_4 at a constant temperature of 303 K. To well know the interaction mechanisms between the inhibitor and metal surface, two prominent adsorption isotherm models, Langmuir and Freundlich, are employed. These models provide useful insights into the ME inhibitor's effectiveness and adsorption behavior over time, shedding light on how the inhibitor interacts with the steel surface to reduce corrosion in acidic circumstances.The adsorption isotherm models for the ME inhibitor, analyzed through the Freundlich and Langmuir models at 303 K, reveal significant insights into the adsorption behavior over different time intervals (12, 24, and 48 hours),[28] as shown in **Figure 6a-b**.

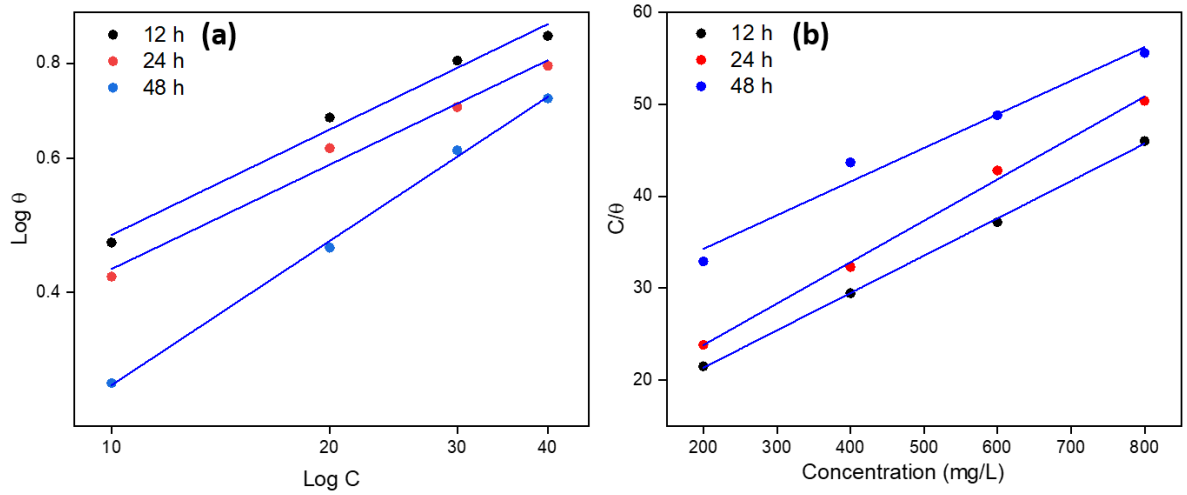

Fig. 6. (a) Freundlich adsorption isotherm, and **(b)** Langmuir adsorption isotherm for MS employing different ME inhibitor doses in 1 M H_2SO_4 solution at 303K.

The Freundlich isotherm give the idea that the adsorption occurs on a heterogeneous surface, where the degree of adsorption increases with concentration but at a diminishing rate. The slope values (1/n) are between 0.46 and 0.63, which indicate favorable adsorption conditions, as depicted in **Figure 6a**. However, the intercept values decrease over time, from -0.78329 at 12 hours to -1.15001 at 48 hours, reflecting a reduction in overall adsorption capacity. The high R^2 values (ranging from 0.97751 to 0.99808) indicate that the Freundlich model fits the data well, highlighting a strong correlation between experimental and predicted surface coverage values.

Table 5. Adsorption isotherm models of ME inhibitors with slope, intercept, and R^2 values derived from weight loss observations at 303K.

Time (h)	Freundlich isotherm $\log \theta = \log K + \frac{1}{n} \log C$			Langmuir isotherm $\frac{C}{\theta} = \frac{1}{K} + C$		
	Slope	Intercept	R^2	Slope	Intercept	R^2
12	0.46065	-0.78329	0.98451	0.04063	13.2259	0.99915
24	0.45596	-0.82338	0.97751	0.04505	14.8092	0.99654
48	0.62989	-1.15001	0.99808	0.03658	26.96291	0.97577

On the other hand, the Langmuir isotherm assumes uniform adsorption sites and suggests that adsorption occurs on a finite number of available sites. The Langmuir model's high R^2 values (0.99915 at 12 hours, 0.99654 at 24 hours, and 0.97577 at 48 hours) suggest that it provides a better fit to the data over time, implying that the adsorption follows a more structured process, as depicted in **Figure 6b**. However, the decrease in slope and increase in intercept over time (from 13.2259 at 12 hours to 26.96291 at 48 hours) suggest that adsorption sites become less available as the process progresses, possibly due to saturation. Overall, both isotherm models show a good fit to the experimental data, with Langmuir providing a more consistent reflection of the adsorption process over time. This indicates that while the ME inhibitor adsorption is favorable and follows a structured model, changes in surface site availability or saturation may affect the process as time advances.

3.5 UV characterization

The **Figure 7** shows the UV analysis of MS coupons in presence and absence of 1M H_2SO_4 solution containing 40 mg/L ME inhibitor at 303K. This study sheds light on how the ME inhibitor inhibits corrosion by establishing a protective layer on the steel surface in the presence of an acidic media[29].

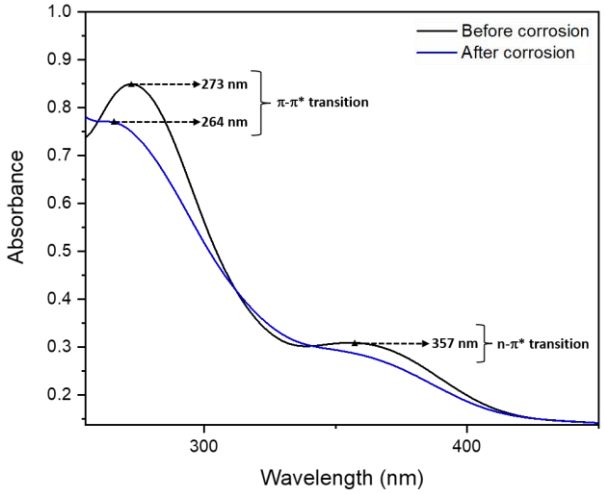

Fig. 7. At 303 K, UV analysis of MS coupons in a 1 M H_2SO_4 solution containing 40 mg/L of ME inhibitor

Table 6 displays the UV parameters for MS both prior to and following immersion in a 1 M H_2SO_4 solution containing a ME inhibitor at a concentration of 40 mg/L at 303 K. The UV spectrum of the mild steel before immersion reveals two prominent peaks one at 273 nm with an absorbance of 0.849 and another at 357 nm with an absorbance of 0.309.

After immersion in a 1 M H_2SO_4 solution containing the ME inhibitor, significant changes were observed in the UV spectrum. The absorbance peak at 273 nm shifted to 264 nm, with a reduced absorbance value of 0.771, indicating that corrosion has impacted the steel surface. This alteration suggests that the oxide layer has dissolved, affecting how MS interacts with UV light. Additionally, the disappearance of the second peak at 357 nm implies that the corrosion process has caused the breakdown of organic compounds or impurities on the steel surface. This loss may also result from chemical interactions between the steel, sulfuric acid, and the ME inhibitor, which modify or degrade the surface species responsible for this absorbance. These spectral changes highlight the inhibitor's role in altering the corrosion process, potentially forming a protective barrier that mitigates further surface deterioration and enhances corrosion resistance.

Table 6. MS UV values both presence and absence in a 1 M H_2SO_4 solution containing 40 mg/L of ME inhibitor at 303 K.

Before immersion		After immersion	
λ_{max} (nm)	Absorbance	λ_{max} (nm)	Absorbance
273	0.849	264	0.771
357	0.309	-	-

The observed alterations in the UV spectra reveal the corrosion mechanisms taking place in an acidic environment. The highly corrosive nature of the 1 M H_2SO_4 solution results in the breakdown of the steel's protective oxide layer, which allows fresh metal to be exposed to corrosion, leading to the generation of soluble iron ions and hydrogen gas. The presence of the ME inhibitor seems to mitigate corrosion by forming a protective layer on the steel surface, which reduces iron solubility and limits hydrogen ion production. The reduction in absorbance at 273 nm and the lack of a peak at 357 nm suggest that both the corrosion process and the inhibitor's effects significantly modify the surface characteristics of the steel. These findings indicate that the ME inhibitor effectively decelerates corrosion by altering surface interactions within an acidic medium. By establishing a protective barrier, the ME inhibitor not only prevents further corrosion but also enhances the lifespan and durability of MS in aggressive environments.

3.6 Contact angle analysis

The **Figure 8** illustrates the notable variations in surface interactions with water that are revealed by the contact angle measurements of MS coupons under various situations. The contact angle for the new MS coupon was 72.51°, which suggests that its surface is moderately hydrophilic. This demonstrates that, untreated metal surfaces, the steel's natural oxide layer permitted some water interaction. The contact angle upto 85.87° presence of 1 M H_2SO_4 solution containing 40 mg/L of ME inhibitor, suggesting the growth of a protective layer on the steel surface. Because this layer prevented the steel from coming into touch with the acidic solution, it reduced the hydrophilicity of the surface and, consequently, the steel's vulnerability to corrosion. The inhibitor altered the surface chemistry of the steel, making it less reactive in the acidic environment. This reduction in

hydrophilicity is indicative of the inhibitor's role in forming a barrier that shields the metal from aggressive corrosion, confirming its efficacy in enhancing corrosion resistance.

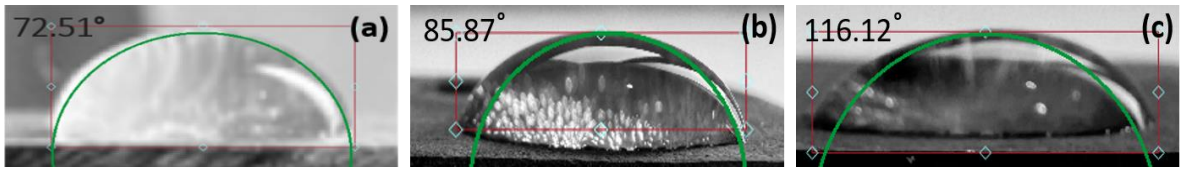

Fig. 8. Contact angle images of MS coupons, **(a)** fresh MS coupon, **(b)** MS coupon in 1 M H_2SO_4 solution with ME inhibitor (40 mg/L), and **(c)** MS coupon in 1 M H_2SO_4 solution.

In contrast, the contact angle surged to 116.12° when the MS coupon was submerged in the sulfuric acid solution without the inhibitor. This marked increase in hydrophobicity was indicative of extensive corrosion, where the oxide layer was dissolved, and the surface became rougher and more uneven leading to the formation of corrosion products. The rough surface texture increased the water-repellent properties, as hydrophobicity is often associated with surface roughness. These observations confirm that the ME inhibitor played a crucial role in modifying the steel surface, reducing corrosion, and enhancing stability by creating a more hydrophobic, less reactive surface in the acidic solution. Without the inhibitor, corrosion significantly altered the surface, increasing its hydrophobicity due to the dissolution of protective layers and the formation of corrosion-induced irregularities.

3.7 SEM Analysis

The surface morphology of MS coupons was examined using the SEM technique, offering detailed images of their microstructural characteristics to evaluate both corrosion damage and the protective impact of the inhibitor [30], as shown in **Figure 9**. In **Figure 9a**, the MS coupon is shown in its fresh, untreated state. The surface is smooth, with visible scratches from the polishing process, which is normal for any freshly polished metal. Since it has not been exposed to any corrosive environment yet, there are no signs of corrosion or damage. This gives us a clear reference point for comparing the effects of corrosion under different conditions.

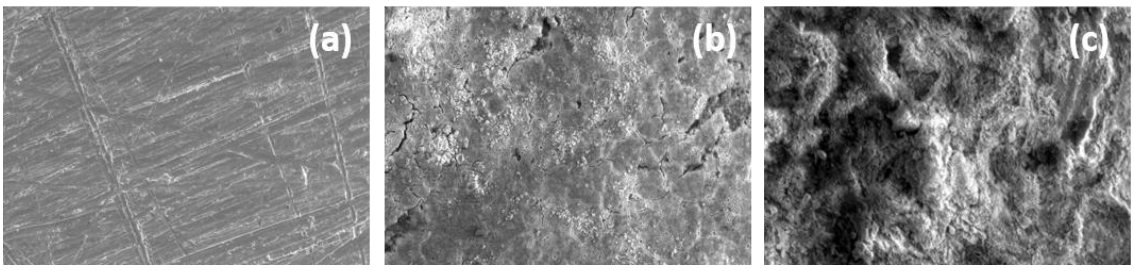

Fig. 9. The SEM images of MS coupons; **(a)** fresh MS coupon, **(b)** in the presence of inhibitor (at a concentration of 40 mg/L) in 1 M H_2SO_4 solution for 24 hours, and **(c)** in 1 M H_2SO_4 solution for 24 hours.

The SEM image in **Figure 9b** displays the MS coupon injected with the ME inhibitor for 24 hours at a concentration of 40 mg/L in 1 M H_2SO_4. Here, the surface is noticeably better than the untreated coupon that was subjected to the acidic solution. While some roughness remains, the level of corrosion is greatly decreased. This shows that the ME inhibitor acts as a defensive coating on the steel surface, avoiding direct contact between the metal and harsh acidic environment. The inhibitor molecules most likely attach onto the metal surface, decreasing acid corrosion. The smoother surface texture suggests that the inhibitor is important in keeping steel's structural integrity, reducing corrosion, and maintaining the material's condition over time.

When immersing the MS coupon in 1 M H_2SO_4 solution without an inhibitor, as seen in **Figure 9c**, the acid's effect on the steel is immediately noticeable. The surface becomes much rougher, with visible corrosion pits and an irregular texture. These pits indicate significant material loss, which is typical when metals are exposed to strong acids without protection. The damage is severe, and such degradation could compromise the structural integrity of the material, leading to potential failure. This image highlights the need for protective measures in acidic environments, where corrosion happens quickly and aggressively.

These results highlight the vital role of corrosion inhibitors in safeguarding metals against the damaging effects of aggressive environments. In situations where corrosion could lead to significant material loss, in industries using acidic solutions, the ME inhibitor plays a vital role in safeguarding the metal. The effectiveness of the ME inhibitor shows how it can be a cost-effective solution to minimize corrosion, improve the durability of steel components, and reduce maintenance costs.

3.8 Comparison of with other natural corrosion inhibitors for MS in acidic media

The **Table 7** presents a comparative analysis of the corrosion inhibition efficiencies of ME extract and other plant-based natural inhibitors for MS in acidic media. The ME extract, obtained using methanol as the solvent, exhibited a notable IE of 86.93% in 1 M H_2SO_4, underscoring its potential as an effective green inhibitor. When compared with other natural inhibitors, such as *Cryptocarya nigra* (91% in 1 M HCl), *Eucalyptus* (88% in 1 M HCl), *Saraca ashoka* (93.09% in 0.5 M H_2SO_4), and *Zingiber officinale* (92.5% in 1 M HCl), *Myrica esculenta* shows slightly lower efficiency. However, it is important to note that inhibition efficiency is strongly influenced by both the nature of the extract and the corrosive medium.

Table 7. Comparison of inhibition efficiency of ME extract with other natural corrosion inhibitors for MS in acidic media.

Plant Extract	Extraction Solvent	Corrosive Medium	Inhibition Efficiency (%)	Ref.
Cryptocarya nigra	Hexane, dichloro-methane, methanol	1M HCl	91	[31]
Eucalyptus	water	1M HCl	88	[32]
Saraca ashoka	water	0.5M H_2SO_4	93.09	[33]
Zingiber officinale	methanol	1M HCl	92.5	[34]
Myrica esculenta	methanol	1M H_2SO_4	86.93	This work

Despite the slightly lower inhibition value, the performance of ME in sulfuric acid medium is promising, particularly considering its eco-friendly nature, availability, and ease of extraction. These findings highlight its potential for further optimization and application in sustainable corrosion prevention strategies.

3.9 Proposed mechanism

The proposed mechanism illustrated in **Figure 10** explains the corrosion inhibition behavior of ME extract on MS in an acidic environment. The mechanism can be understood through the interaction of phytochemical constituents of the extract with the metal surface and the ions present in the corrosive medium.

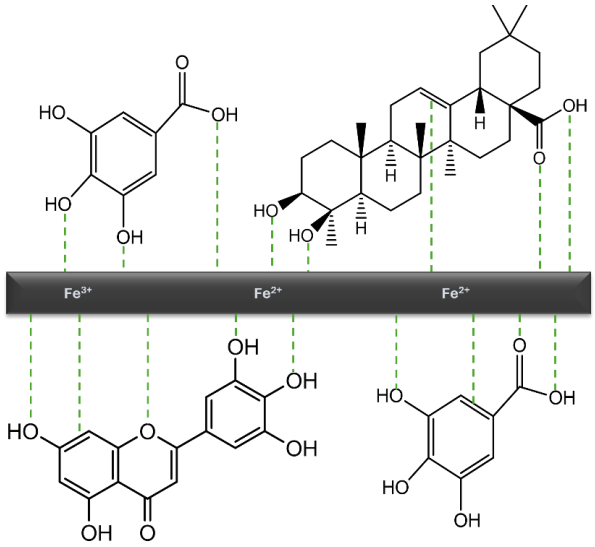

Fig. 10. Proposed mechanism of corrosion inhibition for MS in acidic medium using ME extract as a green inhibitor.

Corrosion of MS in acidic medium primarily occurs due to the oxidation of Fe^0 to Fe^{2+} and subsequently to Fe^{3+}, accompanied by the evolution of hydrogen gas due to the reduction of H^+ ions. The surface of the MS becomes populated with positively charged Fe^{2+} and Fe^{3+} ions, creating active sites prone to aggressive attack by acid molecules. This is where the role of the ME extract becomes crucial.

ME contains various bioactive phytochemicals such as phenolics, flavonoids, tannins, and alkaloids, which possess multiple functional groups like hydroxyl (-OH), carbonyl (C=O), and aromatic rings. These groups have a strong affinity for metal ions and can donate electrons to vacant d-orbitals of Fe atoms, forming coordinate covalent bonds. This leads to the formation of a protective adsorption layer on the MS surface, which effectively blocks the active corrosion sites [32].

As depicted in the **Figure 10**, the molecules from the ME extract are adsorbed onto the MS surface *via* physical or chemical interactions. The dashed green lines symbolize the interaction of lone pair electrons or π-electrons from the inhibitor molecules with the vacant orbitals of Fe atoms on the metal surface. This adsorption creates a barrier that impedes the diffusion of H^+ ions toward the metal surface and retards the anodic dissolution of iron. In conclusion, the ME extract inhibits corrosion by adsorbing onto the metal surface and forming a protective barrier, thereby reducing the electrochemical reactions responsible for corrosion. This eco-friendly and sustainable mechanism offers an effective alternative to toxic synthetic inhibitors commonly used in industrial processes [22].

4. Conclusions

The current study highlights the effectiveness of the ME extract as a corrosion inhibitor for MS in acidic environments. Weight loss studies show a considerable reduction in corrosion, with an inhibitory effectiveness of 86.93% at a 40 mg/L dosage within 12 hours. Electrochemical polarization experiments show a change in the corrosion potential toward more noble values, indicating a reduction in corrosion due to the creation of a protective inhibitor layer. Adsorption studies suggest that the inhibition mechanism involves both monolayer and possible multilayer adsorption on the MS surface. Measuring the contact angle reveals that the ME inhibitor increases the surface's hydrophobicity, lowering it from 116.12° (corroded MS) to 85.87°, a sign that a stable protective layer has formed. The effectiveness of the inhibitor is further supported by UV spectroscopy, which shows a shift in peak wavelengths and a decrease in absorbance, demonstrating the creation of a protective layer. Ultimately, SEM research shows a notable decrease in pitting and surface damage, maintaining the steel's structural integrity. Thus, the ME inhibitor turns out to be a very efficient and environmentally beneficial mild steel corrosion inhibitor in acidic environments.

Acknowledgments

The authors are grateful to Department of Chemistry, Chandigarh University, Gharuan, Punjab, India for providing all the facilities to carry out the research.

Author Contributions

Abhishek Sharma – writing-original draft; Navneet Kaur – visualization, writing-review and editing; Manvinder Kaur – investigation, methodology, conceptualization; Rajeev Sharma – investigation; and Harvinder Singh Sohal – supervision, methodology, project administration, and resources.

References and Notes

[1] Javaherdashti, R. *Anti-Corrosion Methods Mater.* **2000**, *47*, 30. **[Crossref]**

[2] Biezma, M. V.; San Cristóbal, *J. R. Corros. Eng. Sci.*

Technol. **2005**, *40*, 344. [Crossref]

[3] Cole, I. S.; Marney, D. *Corros. Sci.* **2012**, *56*, 5. [Crossref]

[4] Eddy, N. O. *Int. J. Phys. Sci.* **2009**, *4*, 165.

[5] Singh, A.; Ebenso, E. E.; Quraishi, M. A. *Int. J. Corros.* **2012**, 897430. [Crossref]

[6] Haldhar, R.; Prasad, D.; Saxena, A.; Kumar, R. *Sustain. Chem. Pharm.* **2018**, *9*, 95. [Crossref]

[7] Peter, A.; Obot, I. B.; Sharma, S. K. *Int. J. Ind. Chem.* **2015**, *6*, 153. [Crossref]

[8] Döner, A.; Kardaş, G. *Corros. Sci.* **2011**, *53*, 4223. [Crossref]

[9] Dehghani, A.; Bahlakeh, G.; Ramezanzadeh, B.; Ramezanzadeh, M. *J. Mol. Liq.* **2019**, *279*, 603. [Crossref]

[10] Kabra, A.; Sharma, R.; Singla, S.; Kabra, R.; Baghel, U. S. *J. Ayurveda Integr. Med.* **2019**, *10*, 18. [Crossref]

[11] Chahul, H.; Danat, T.; Wuana, R. *J. Mater. Environ. Sci.* **2019**, *10*, 266.

[12] Bhatt, I. D.; Rawal, R. S.; Dhar, U. *Mt. Res. Dev.* **2000**, *20*, 146. [Crossref]

[13] Kabra, A.; Martins, N.; Sharma, R.; Kabra, R.; Baghel, U. S. *Plants* **2019**, *8*, 149. [Crossref]

[14] Yadav, A. et al. *Polymers* **2023**, *15*, 4339. [Crossref]

[15] Parmar, R. G. B. Y. S. et al. *Pharma Innov. J.* **2022**, *11*, 1616.

[16] Bhatt, S. C. et al. *Food Chem. Adv.* **2023**, *3*, 100434. [Crossref]

[17] Shah, H.; Naseer, A.; Gupta, N.; Patil, S. M.; Upadhyay, S. K.; Singh, R. *Plant Cell Biotechnol. Mol. Biol.* **2021**, *22*, 90.

[18] Dua, T. K. et al. *Molecules* **2021**, *26*, 258. [Crossref]

[19] Shri, P. S. R. *Indian J. Pharm. Sci.* **2018**, 80. [Crossref]

[20] Jeeva, S.; Lyndem, F. G.; Sawian, J. T.; Laloo, R. C.; Mishra, B. P. *Asian Pac. J. Trop. Biomed.* **2011**, *1*, S174. [Crossref]

[21] Khadraoui, A. et al. *J. Mol. Liq.* **2016**, *216*, 724. [Crossref]

[22] Chaudhary, S.; Tak, R. K. *Biointerface Res. Appl. Chem.* **2022**, *12*, 2603. [Crossref]

[23] Adejo, S. O. IOSR *J. Appl. Chem.* **2014**, *6*, 66. [Crossref]

[24] Shamsuzzaman, M.; Kalaiselvi, K.; Prabakaran, M. *Appl. Sci.* **2021**, *11*, 10150. [Crossref]

[25] Salleh, S. Z. et al. *J. Clean. Prod.* **2021**, *304*, 127030. [Crossref]

[26] Miralrio, A.; Vázquez, A. *E. Processes* **2020**, *8*, 942. [Crossref]

[27] Dehghani, A.; Bahlakeh, G.; Ramezanzadeh, B. *Bioelectrochemistry* **2019**, *130*, 107339. [Crossref]

[28] Saxena, A.; Prasad, D.; Haldhar, R.; Singh, G.; Kumar, A. *J. Mol. Liq.* **2018**, *258*, 89. [Crossref]

[29] Gadow, H. S.; Motawea, M. M. *RSC Adv.* **2017**, *7*, 24576. [Crossref]

[30] Shah, H.; et al. *Plant Cell Biotechnol. Mol. Biol.* **2021**, *22*, 90.

[31] Ahanotu, C. C.; Ezigbo, V. O.; Okonkwo, S. *I. J. Mater. Environ. Sci.* **2024**, *2*, 251.

[32] Ituen, E.; Akaranta, O.; James, A. *Chem. Sci. Int. J.* **2017**, *18*, 1. [Crossref]

[33] Isimjan, T. T.; Wang, T.; Rohani, S. *Chem. Eng. J.* **2012**, *210*, 182. [Crossref]

[34] de la Fuente, D.; Díaz, I.; Simancas, J.; Chico, B.; Morcillo, *M. Corros. Sci.* **2011**, *53*, 604. [Crossref]

How to cite this article

Sharma, A.; Kaur, N.; Kaur, M.; Sharma, R.; Sohal, H. S. *Orbital: Electron. J. Chem*. **2025**, *17*, 426. DOI: http://dx.doi.org/10.17807/orbital.v17i5.22789